Automated Planning of Scan Geometry in Follow-up Prostate MRI Examinations

Peter Mazurkewitz[1], Daniel Bystrov[1], Peter Koken[1], Torbjoern Vik[1], and Julien Sénégas[1]
[1]*Philips Research Laboratories, Hamburg, Germany*

Purpose: When reading MR-images of a follow-up prostate examination, it is often required to compare slice by slice the images of the initial (denoted thereafter as baseline) and follow-up scans, for example to analyze the growth of a tumor for patients under active surveillance. For this purpose, it is highly desirable to acquire the images of the follow-up scans in the exact same geometry with respect to the target anatomy as in the baseline scans, as previously demonstrated for the brain [1, 2]. Manual planning of follow-up prostate scans can be very time consuming and its accuracy is operator dependent. Therefore, in this work we present a fully automated method for robust and accurate planning of follow up prostate scans. In order to better cope with the specific challenges of prostate MR exams, where high-resolution scans with small FOV generally need to be planned, the rigid registration method originally presented in [2] and [4] was adapted by using an image based organ detection [3] as initialization of the registration algorithm. This new approach was evaluated retrospectively on volunteer data and tested prospectively on a commercial MRI system.

Methods: The proposed planning method consists of two steps: 1) Detection of the approximate location of the prostate center in a 3D survey using a 3D image-based classifier and extraction of a corresponding region-of-interest (ROI) with reduced FOV, 2) Rigid registration between the baseline image and the cropped 3D survey to determine the geometry transformation defining the scan plan. The robustness and accuracy of this approach was first investigated by retrospectively analyzing baseline data that were acquired in 20 healthy volunteers on a 3T clinical scanner (Ingenia, Philips Healthcare) with a 32-element body coil. A routine prostate protocol was used, consisting of the following sequences: **1.** T1 weighted TSE (voxel size = 0.8 x 1.0 x 3.0 mm^3, FOV in LR-AP-FH = 180 x 180 x 83.5 mm^3, axial orientation), **2.** T2 weighted TSE (voxel size = 0.7 x 0.7 x 3.0 mm^3, FOV in LR-AP-FH = 180 x 180 x 83.5 mm^3, axial orientation), **3.** T2 weighted TSE (voxel size = 0.8 x 1.1 x 3.0 mm^3, FOV in LR-AP-FH= 71 x 180 x 180 mm^3, sagittal orientation). 3D surveys using a balanced FFE sequence (TR / TE = 2.9 / 1.41 ms, flip angle = 15°, voxel size = 2.0×2.0×3.0 mm^3, FOV = 450×450×300 mm^3, transversal orientation, total acquisition time 41s) were acquired twice during the same session: one for planning at the beginning, and one at the end of the imaging session, after controlled repositioning of the volunteer to increase the number of training data for the organ detection algorithm. The survey data of 15 volunteers were used to train the prostate detection algorithm, following the approach presented in [3]. For each contrast type, the geometry plans computed retrospectively with the proposed method on the basis of the initial survey were compared to the plans used for acquisition, assuming negligible patient motion between the acquisition of the survey and the consecutive scans. The residual translation as well as the mean residual absolute displacement over the entire imaged volume was computed to characterize the planning accuracy.
In addition, follow-up imaging sessions were performed approx. 4 months after the baseline scans in three volunteers using the same routine protocol and the proposed planning approach. The images of the three corresponding baseline diagnostic scans were transferred back to the image database of the MR system. The imaging session started with the acquisition of a 3D survey using the above described balanced FFE sequence. Then, the prostate detection and image registration process started automatically in the background and the three scans were acquired with the automatically computed geometry plan, after quality review and confirmation by the operator. The whole planning process was completed within a few seconds, during acquisition of a B1 reference scan, and thus, did not prolong the total imaging session time in these cases. No further planning step was required to complete the examination.

Results and Discussion: In one data set, the prostate detection failed. The remaining 19 data sets were used for the retrospective evaluation. Table 1 shows the accuracy results for each contrast type. For comparison, the detection error, measured between the detected prostate center and the center of the true geometry plan, was computed. A slight detection bias towards the posterior and foot direction can be noted, which was largely reduced after the rigid registration. Mean overall residual planning errors were between 3 and 4 mm.
The three volunteer follow-up imaging sessions were performed successfully, with no need to manually correct the automatically computed geometry. Fig. 1 shows one example of baseline / follow-up scans in the same slice position for a selected volunteer, visually demonstrating the good alignment achieved by the planning algorithm. Fig. 2 illustrates the intermediate step with the detection of the prostate center.

Conclusions: In this volunteer study, the proposed method allowed to largely simplify the examination workflow while achieving admissible accuracy in alignment. Previous attempts to apply directly the registration algorithm between the 3D survey and the baseline scans failed to be robust, due to the very different FOV and the existence of local deformations making the rigid registration problem relatively ill-posed. The use of an image classifier to detect the prostate center allowed solving these problems by yielding a suitable initialization and by reducing the extent of the search range. Further investigation is required to train the image classifier on a larger, clinical database and to assess whether the current accuracy is good enough for clinical applications, especially for quantitative analysis.

References: [1] Sénégas et al., ISMRM 2012 proc. 2567 [2] Koken et al., ISMRM 2012 proc. 2774 [3] Demarcy et al. ISMRM 2014 proc. 0411 [4] Sénégas et al., ISMRM 2013 proc. 2588

Figure 1: Image data of a selected volunteer. Left: baseline examination, right: corresponding slice of follow-up examination (up: T2W TSE, mid: T1W TSE, below: survey showing different volunteer positions)

Scan	Detection Error (mm)			Final Residual Error (mm)			
	L-R	A-P	F-H	L-R	A-P	F-H	Overall Displ.
T1W_TSE_ax	1.3±2.3	7.3±6.1	-4.9±10.0	-0.9±0.7	2.7±1.0	-2.2±1.2	3.9±1.2
T2W_TSE_ax	1.3±0.4	7.3±6.1	-4.9±10.0	-0.8±0.5	1.7±0.6	-1.7±0.6	2.7±0.7
T2W_TSE_sag	1.2±2.3	7.5±5.0	-7.6±11.4	0.7±0.7	1.6±0.9	-1.6±2.2	3.0±1.7

Table 1: Mean and standard deviation of residual translation and overall displacement for the three sequences used in the retrospective volunteer study.

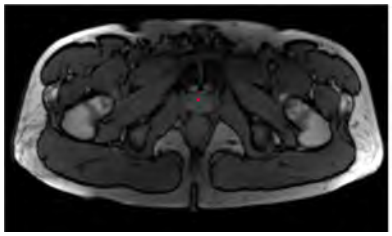

Figure 2: result of the prostate detection (red point)